Modeling proton intensity gradients and radiation dose equivalents in the inner heliosphere using EMMREM: May 2003 solar events

M. A. Dayeh,[1] M. I. Desai,[1,2] K. Kozarev,[3] N. A. Schwadron,[4] L. W. Townsend,[5] M. PourArsalan,[5] C. Zeitlin,[6] and R. B. Hatcher[5]

Received 31 December 2009; revised 30 June 2010; accepted 6 July 2010; published 18 November 2010.

[1] Solar energetic particles (SEPs) provide a significant radiation hazard for manned and unmanned interplanetary (IP) space missions. In order to estimate these hazards, it is essential to quantify the gradients of SEP intensities in the IP medium. The Earth-Moon-Mars Radiation Exposure Module (EMMREM) is a new project aimed at characterizing the time-dependent radiation exposure in IP space. In this paper, we utilize EMMREM to study the radial dependence of proton peak intensities, event fluences, and radiation dose equivalents of 27–31 May 2003 SEP events at eight different locations between 1 and 4.91 AU at energies between ~1.5 MeV and ~130 MeV. We have modeled onset times and intensity profiles of the SEP events at Mars and Ulysses and found very good agreement at different energies. We report observations of energetic particles at locations with magnetic field line footprints that are separated by ~90° in heliolongitude, possibly indicating very large coronal mass ejection sizes and/or high cross-field diffusion at large radial distances. Our results show that radial dependencies of proton peak intensities exhibit a broken power law between 1 to 2.5 AU and 2.5 to 4.91 AU, ranging between $R^{-2.52 \pm 0.42}$ and $R^{-5.97 \pm 0.32}$ for 25 MeV and between $R^{-2.13 \pm 0.36}$ and $R^{-5.21 \pm 0.29}$ for 52 MeV, where R is the radial distance from the Sun in units of AU. Event fluences exhibit a similar behavior but with a harder spectra. Radiation dose calculations show that these events did not pose a short-term radiation hazard to humans in the IP space.

Citation: Dayeh, M. A., M. I. Desai, K. Kozarev, N. A. Schwadron, L. W. Townsend, M. PourArsalan, C. Zeitlin, and R. B. Hatcher (2010), Modeling proton intensity gradients and radiation dose equivalents in the inner heliosphere using EMMREM: May 2003 solar events, *Space Weather*, *8*, S00E07, doi:10.1029/2009SW000566.

1. Introduction

[2] The interplanetary (IP) space environment is characterized by intense energetic radiation that poses serious hazards to astronauts and instrumentation alike. Once space missions cross beyond the Earth's natural protective shields, the atmosphere and the magnetosphere, they become fully exposed to the harsh IP radiation environment. The two main sources of high-energy particles in IP space are galactic cosmic rays (GCRs) and solar energetic particles (SEPs). GCRs are energetic particles of galactic origin that are able to propagate into the inner solar system. They consist of protons and heavy nuclei with energies extending up to tens of GeV/amu and beyond. Although they are very hard to shield against, GCR radiation in the heliosphere is continuous and varies over long time scales (years), depending on the phase of solar activity [e.g., *Le Roux and Potgieter*, 1995]. For short-duration space missions, shielding against GCRs has been ignored so far. However, this is not the case for long-duration and deep space missions, where astronauts could reach their career limit of radiation exposure in just about 3 years [*Cucinotta et al.*, 2001]. On the other hand, SEPs are bursts of energetic particles of solar origin with intensities up to 5 orders of magnitude above the observed GCR intensities (e.g., the

[1]Space Science and Engineering Division, Southwest Research Institute, San Antonio, Texas, USA.
[2]Department of Physics and Astronomy, University of Texas at San Antonio, San Antonio, Texas, USA.
[3]Department of Astronomy, Boston University, Boston, Massachusetts, USA.
[4]Institute for the Study of Earth, Oceans, and Space, University of New Hampshire, Durham, New Hampshire, USA.
[5]Department of Nuclear Engineering, University of Tennessee, Knoxville, Tennessee, USA.
[6]Space Studies Department, Southwest Research Institute, Boulder, Colorado, USA.

Bastille Day SEP event of year 2000 [see also *Mewaldt et al.*, 2007]). SEPs in the heliosphere are unpredictable, highly variable, and in some cases intense enough to permanently damage spacecraft electronics and pose a potential lethal risk to astronauts within time scales of days [*Wilson et al.*, 1997].

[3] With the current NASA *Vision for Space Exploration* of returning astronauts to the Moon and sending manned missions to Mars, it is of crucial importance to understand and develop appropriate mitigation strategies for the hazardous radiation in the IP medium. Enhancing our understanding of particle propagation in the heliosphere will enable us to predict the variations of SEP intensities and associated radiation doses at different heliospheric radial and longitudinal locations. This is a key factor that will help us optimize astronaut protection and instrument radiation shielding.

[4] Substantial effort has already been made to study the propagation and radial gradients of SEP intensities and fluences in the heliosphere [e.g., *Hamilton et al.*, 1990; *Shea*, 1988; *Ng and Reames*, 1994; *Boufaida and Armstrong*, 1997; *Kallenrode*, 1993; *Smart and Shea*, 2003; *Ruzmaikin et al.*, 2005; *Foullon et al.*, 2005; *Lario et al.*, 2006, 2007; *Denker et al.*, 2007]. However, the scarcity of simultaneous SEP measurements by multiple spacecraft at different locations in the heliosphere, severely limits our ability to compare observations and model results.

[5] Using a spherically symmetric transport model [*Parker*, 1965], *Hamilton* [1988] studied the radial dependence of SEP peak intensities and fluences in heliosphere including spatial diffusion, convection, and adiabatic energy loss effects while ignoring the focusing of energetic particles along the magnetic field lines.

[6] This model was applied on measured energetic proton intensities (10–70 MeV) in order to extrapolate SEP intensities to distances less and beyond 1 AU [*Shea*, 1988]. A workshop held at the Jet Propulsion Laboratory in 1987 [*Feynman and Gabriel*, 1988] discussed this descriptive model and concluded with consensus a set of recommendations for radial extrapolations of peak particle fluxes and SEP fluences at different radial distances [see also *Lario et al.*, 2006, 2007]. These recommendations are (1) for flux extrapolations from 1 to > 1 AU, use a functional form of $R^{-3.3}$ and expect variations ranging from R^{-4} to R^{-3}; (2) for flux extrapolations from 1 to < 1 AU, use a functional form of R^{-3} and expect variations ranging from R^{-3} to R^{-2}; and (3) for fluence extrapolations from 1 AU to other distances, use a functional form of $R^{-2.5}$ and expect variations ranging from R^{-3} to R^{-2}. Here R is the radial distance from the Sun in units of AU. *Smart and Shea* [2003] later reported that these generalizations apply only to specific types of magnetically connected SEP events, a case that is not necessarily true for large SEP events, where particles are mostly accelerated diffusively at coronal mass ejection (CME) driven IP shocks [e.g., *Li et al.*, 2005]. Recent models of particle acceleration by traveling IP shocks have shown that the observer shock magnetic connectivity and the continuous acceleration of particles at the shock have direct consequences on SEP intensity profiles and energy spectra at different heliospheric distances [e.g., *Zank et al.*, 2000; *Rice et al.*, 2003; *Li et al.*, 2003; *Luhmann et al.*, 2007]. This in turn affects the radial dependences of both peak fluxes and fluences [e.g., *Aran et al.*, 2005b; *Ruzmaikin et al.*, 2005].

[7] More recently, using data from Helios 1 and Helios 2 and IMP 8, *Lario et al.* [2006] studied the radial and longitudinal dependence of proton peak intensities and fluences in 72 SEP events between 0.3 and 1 AU. They found that the radial dependencies are less steep than those recommended by the JPL workgroup consensus concluding that energetic particles radial dependencies based on classical geometries overestimate particle fluxes at distances R < 1 AU. A summary of the work done by other researchers studying radial dependence of SEP intensities and fluences in the inner heliosphere (<1 AU) is detailed by *Lario et al.* [2006].

[8] In general, the classical view of scaling intensities and fluences with radial distances yields in R^{-3} and R^{-2} dependences for intensities and fluences, respectively, where particles are assumed to be confined to a flux tube that expands as a function of radial distance from the sun. However, we now know that this is not the case with all SEP events. CME-driven IP shocks accelerate SEPs continuously as they propagate and their radial profiles become dependent not only on the radial distance, but also on particle energies, acceleration efficiency, and shock parameters [*Aran et al.*, 2005a; *Ruzmaikin et al.*, 2005; *Lario et al.*, 2007].

[9] During the last two decades, observations of SEP events from spacecraft at different radial heliospheric distances (e.g., Helios A and B, 0.3 AU; ACE, 1 AU; Ulysses, 5 AU, etc.) have shaped our understanding of SEP transport in the heliosphere. At radial distances close to the sun (<1 AU, Helios spacecraft observations), multiple SEP events can be easily identified from their time scales since they did not yet expand enough to possibly merge into a larger structure. In the near-Earth orbit, these events could still be identified individually by their time scales, nonetheless, effects of transport propagation and velocity dispersion can also be observed and SEP events that are small enough could be over shadowed by the larger ones. Farther away from the Sun where the IP magnetic field becomes more azimuthally pronounced, the time profiles of SEP intensities are broader and it becomes harder to identify individual SEP events. Additionally, CMEs may interact and merge as they propagate in the IP medium [*Burlaga et al.*, 2002; see also *Boufaida and Armstrong*, 1997; *Reames*, 1999]. It has also been shown that the propagation of SEPs is significantly affected by solar wind structures, magnetic field regions, and heliospheric sector boundaries [e.g., *Reames*, 2001; *Barouch and Burlaga*, 1976; *Lario et al.*, 2001, 2008; *Qin and Li*, 2008]. Subsequently, SEP profiles are always modulated and altered by IP propagation effects at large heliospheric distances and thereby making it more difficult to trace them back spatially and temporally to their progenitors on the Sun [see also *Richardson et al.*, 2006; *Kallenrode*, 2005].

[10] A new project, The Earth-Moon-Mars Radiation Exposure Module (EMMREM), has been recently developed aimed at characterizing the time-dependent radiation exposure in IP space environments [*Schwadron et al.*, 2010; *Kozarev et al.*, 2010]. EMMREM consists of two major workhorses, a 3-D energetic particle diffusive transport code (Energetic Particle Radiation Environment Module (EPREM)) and a space radiation transport code (a modified version of Baryon Transport Model (BRYNTRN) [*Wilson et al.*, 1988, 1991]). In this paper, we utilize EMMREM to study the radial and longitudinal dependence of proton peak intensities, event fluences, and radiation dose equivalents (for various aluminum and water shield thicknesses) of SEPs at eight different locations between 1 and 5 AU. We use proton measurements from Solar and Heliospheric Observatory (SOHO) Energetic and Relativistic Nucleon and Electron experiment (ERNE) [*Torsti et al.*, 1995] at energies between ~1.5 MeV and ~130 MeV during the 27–31 May 2003 SEP events as a model input and compare the results of EMMREM at two energy channels, 25 MeV and 52 MeV, to proton measurements by spacecraft at Mars and Ulysses, located at radial distances of 1.44 and 4.91 AU, and longitudes of 202.1° and 78.5°, respectively.

[11] In sections 2, 3, and 4 we describe the data sources, event selection, and observations at Earth, Mars, and Ulysses locations, respectively. In section 5, we briefly describe the EMMREM module and input parameters. In sections 6 and 7 we present EMMREM predictions and compare them with observations. In section 8 we discuss the results and conclude the analyses.

2. Instrumentation

[12] Data presented in this study were acquired from different instruments on board spacecraft at different heliospheric locations. At 1 AU, we use hourly averaged proton intensities at energies between ~1.5 MeV and ~130 MeV, as measured by ERNE (data available at http://www.srl.utu.fi/erne_data/) [*Torsti et al.*, 1995] on board the SOHO spacecraft, launched in December 1995. ERNE consists of two energy sensors that measure H-Fe at energies extending from few MeV nucleon^{-1} up to few hundreds of MeV nucleon^{-1} (species-dependent). Observations at Mars (at 1.44 AU during this period) were made by the Martian Radiation Environment Experiment (MARIE) [*Zeitlin et al.*, 2004] on board the Mars Odyssey spacecraft, which was launched in April 2001. We use count rates of protons at energies between 16 MeV and 27 MeV. MARIE is an energetic particle spectrometer designed to measure ions in the energy range of 16 MeV nucleon^{-1} to 500 MeV nucleon^{-1}. MARIE operated successfully from March 2002 until October 2003, when it was turned off during the intense Halloween SEP events due to unrecoverable damage. At Ulysses farther out in the heliosphere, we use the pulse height analysis (PHA) and count rate proton data of protons obtained by the High-Energy Telescope (HET) instrument within the Cosmic Ray and Solar Particle Investigation (COSPIN) (see *Simpson et al.* [1992] for a detailed description) consortium onboard the Ulysses spacecraft. In particular, we use 3 h averages from proton channels H3 (count rates; 14.5–41.17 MeV), H4 (PHA; 39–70 MeV) and (PHA; 71–94 MeV). Differential intensities in the lowest-energy channel (H3) are computed by subtracting the preevent background and dividing by the geometric factor for that energy range.

[13] In addition, we use data from the solar wind plasma experiment [*Bame et al.*, 1992] and magnetometer [*Balogh et al.*, 1992] onboard Ulysses, the Solar Wind Electron Proton Alpha Monitor (SWEPAM) [*McComas et al.*, 1998] and the MAG [*Smith et al.*, 1998] instrument on board the Advanced Composition Explorer (ACE) located at the Lagrangian point L1, and the SOHO Large Angle and Spectrometric Coronagraph (LASCO) CME Catalog [*Gopalswamy et al.*, 2009].

3. Event Selection

[14] During the period from 17 May 2003 to 17 December 2004, Ulysses moved from 15° to –15° into southerly latitudes crossing the ecliptic plane in its third and last orbit around the Sun. This near-ecliptic location was ideal to study particle fluxes at different radial distances ignoring the effects of latitudinal transport [e.g., *Fisk and Jokipii*, 1999]. During this period, we searched for SEP events that satisfied the following criteria: (1) the preevent period is quiet at energies above ~20 MeV for at least 7 days at SOHO (1 AU) and Ulysses (~5 AU), leading to an isolated SEP event; (2) SOHO, Odyssey, and Ulysses are more than 100° separated in heliolongitude; (3) proton intensities at ~20 MeV are enhanced by at least an order of magnitude at both locations (SOHO and Ulysses); and (4) intensity enhancements occur at all energies between 2 and 100 MeV at 1 AU during the onset of the SEP event. We note that due to its limited operation time, MARIE measurements are only available through October 2003.

[15] Based on this criterion, we selected a sequence of SEP events that originated from an active region on the western limb of the Sun during May 2003. Particle enhancements associated with these events were observed near Earth (SOHO, 1 AU), Mars (1.44 AU), and Ulysses (4.91 AU). The magnetic footprints of the three observers were close to the ecliptic plane (within ~16°) and covered a large heliolongitude of ~90°.

4. Observations

4.1. The 27–31 May Solar Activity

[16] During the last week of May 2003, an active region (NOAA AR365) developed rapidly into a complex and dynamic magnetic field region with more than 70 visible sunspots (Solar Influences Data Analysis Center bulletin, May 2003; available at http://www.sidc.be/). It became the dominant flare-productive region on the visible solar disc and produced a series of flares with variable class strengths

Table 1. Characteristics of the SEP-Associated CMEs That Originated From NOAA SEC Region AR10365

		Flare[a]			Associated CME[b]		SEP Event[c]		
Event	Date	Peak	GOES Class	Derived EIT Position	First C2 Appearance	Speed (km/s)	Start[d]	Peak	IP Shock Arrival Time[e]
1	27 May 2003	2307	X1.3	S07W16	2350	964	2335	1530	29 May 1155
2	28 May 2003	0027	X3.6	S07W20	0050	1366	—	—	29 May 1825
3	29 May 2003	0105	X1.2	S07W31	0127	1237	—	—	30 May 1600
4	31 May 2003	0224	M9.3	S07W59	0230	1835	0440	0645	—

[a]Latest Events Archive at http://www.lmsal.com/solarsoft/latest_events_archive.html.
[b]SOHO LASCO CME catalog at http://cdaw.gsfc.nasa.gov/CME_list/index.html.
[c]NOAA solar proton events list at http://umbra.nascom.nasa.gov/SEP/seps.html.
[d]Based on enhancements above 10 protons/(cm^2 sr s MeV).
[e]ACE shock list at http://www.bartol.udel.edu/~chuck/ace/ACElists/obs_list.html#shocks.

(C, M, and X). The largest X-ray flare (X3.6) occurred on 28 May, when the magnetic activity reached its maximum [*Chae et al.*, 2004]. Over the course of 4 days (27–31 May), four intense flares associated with halo CMEs were observed at the Sun leading to large enhancements in energetic proton intensities (e.g., GOES and SOHO), and causing geomagnetic and ionospheric disturbances [*Hanuise et al.*, 2006] at Earth. Possible > 10 GeV particle detection in association with these flares using ground-based neutron monitors has been discussed as well [*Sako et al.*, 2005]. Table 1 lists the characteristics of these flares, associated CMEs, SEP events, and IP shocks as measured by different platforms near 1 AU.

4.2. Spatial Distribution of Observers at Earth, Mars, and Ulysses on 28 May 2003

[17] Figure 1a shows the constellation of Earth (SOHO), Mars (Odyssey), and Ulysses in heliographic coordinates on 28 May 0000 UT (day of year (DOY) 148), looking from the north down at ecliptic plane. Nominal magnetic field lines (MFLs) connecting each observer to the Sun are shown using an averaged solar wind speed of 500 km/s measured during the preevent period at 1 AU. Dashed magnetic field lines represent those connected to the origin of the four flares, whose liftoff locations on the solar disc with respect to Earth are indicated. We remark that the four flares occurred within 3 days, thus the spatial configuration of the observers did not change significantly during this short period. The dashed circle represents the Earth orbit.

[18] Figure 1b shows a portion of a Mollweide projection of the Sun (40° on both sides of the solar ecliptic are shown) during 27–31 May 2003. In Figure 1b, we plot the projected heliographic locations of the four flares (observed X-ray peak), Mars, and Ulysses observers on the solar surface as observed from Earth. The footprints of the MFLs connecting all observers are also shown. These were traced back to the solar surface assuming a nominal Parker spiral magnetic field configuration with a constant solar wind speed. The black horizontal arrow crossing through the flare locations depicts the motion of the active region during the 4 day period. Blue, red, and black thick lines indicate the solar magnetic field configuration mapped at 2.5 solar radii from the Sun (obtained by the Wilcox Observatory).

[19] As illustrated in Figure 1b, flare locations and all observers are very close to the ecliptic plane, with all flares launched from a fixed latitude of 7°S, Earth is located at 1.2°S, Mars at 1.35°N, and Ulysses at 14.4°N relative to the ecliptic plane. We assume that out-of-ecliptic propagation effects are negligible in this narrow latitudinal range. As shown, Earth was located in a well-connected position during all 4 days of solar activity, with a maximum of ~31° separation between the footprint of Earth MFL and the farthermost flare location (F1). Mars was located at 1.44 AU from the sun and ~30° (±3° within 3 days) to the west of the Earth in heliolongitude (see Figure 1a). The footprint of Mars MFL is about 82° from F1 and F2, ~66° from F3, and ~38° from F4. Ulysses spacecraft was located at 4.91 AU radially from the Sun and ~92° to the east of the Earth in heliolongitude. Ulysses' MFL footprint was close to all flares in latitude but was significantly apart in heliolongitude from all flare locations and other observers. The closest distance between Ulysses MFL footprint and the flare locations was ~74°, during the 31 May flare, labeled F4 in Figure 1b. Note that the footprints of Earth, Mars, and Ulysses observers are located in the same magnetic hemisphere.

[20] Table 2 lists the locations of the X-ray peak intensities associated with the four flares on the solar disc along with the latitudes, heliolongitudes, MFL footprint heliolongitudes, and radial distances of Earth, Mars, and Ulysses during each of the flares. The differences between MFL footprints of different observers and the location of the four flares are also listed.

4.3. Energetic Particle Observations at Earth, Mars, and Ulysses

[21] Figure 1c shows ~25 MeV proton intensities at 1 AU, 1.44 AU, and 4.91 AU as measured by instruments onboard SOHO, Odyssey, and Ulysses, respectively, during the period from 26 May to 14 June 2003 (DOY 146 to 165). The solar wind, interplanetary conditions, and the timeline of these events from the Sun to 1 AU are detailed by *Hanuise et al.* [2006]. To our knowledge, the implications of these events and the corresponding heliospheric conditions at Ulysses have not been discussed yet and this is not the scope of this paper. However, in a recent survey of inter-

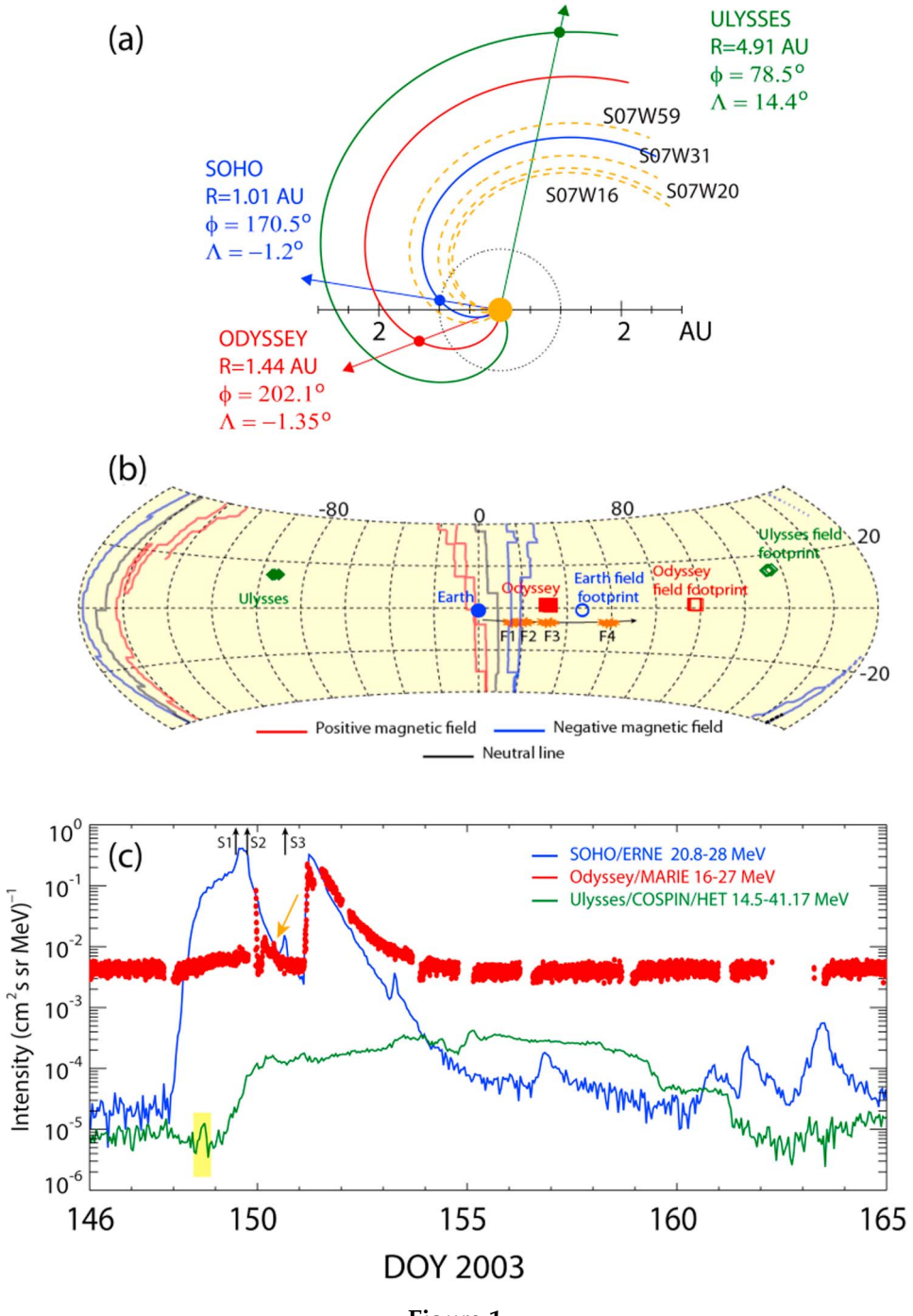
(a)
ULYSSES
R=4.91 AU
ϕ = 78.5°
Λ = 14.4°
S07W59
S07W31
S07W16
S07W20
SOHO
R=1.01 AU
ϕ = 170.5°
Λ = −1.2°
2
2
AU
ODYSSEY
R=1.44 AU
ϕ = 202.1°
Λ = −1.35°
(b)
-80
0
80
20
-20
Ulysses
Earth
Odyssey
Earth field footprint
Odyssey field footprint
Ulysses field footprint
F1 F2 F3
F4
Positive magnetic field
Negative magnetic field
Neutral line
(c)
S1
S2
S3
SOHO/ERNE 20.8-28 MeV
Odyssey/MARIE 16-27 MeV
Ulysses/COSPIN/HET 14.5-41.17 MeV
Intensity (cm^2 s sr MeV)$^{-1}$
10^0
10^{-1}
10^{-2}
10^{-3}
10^{-4}
10^{-5}
10^{-6}
146
150
155
160
165
DOY 2003

Figure 1

Table 2. Longitudinal Properties of the Flares and the Spacecraft (Vsw = 500 km/s)

Observers	L (deg)	ϕ (deg)	$\phi_{\text{footprint}}$ (deg)	$\lvert\phi_{\text{footprint}}-\phi_{\text{Flare}}\rvert$ (deg)	R (AU)
		27 May, 2307 UT (ϕ_{Flare} = 186.50°) and 28 May, 0027 UT (ϕ_{Flare} = 190.5°)			
SOHO	−1.2	170.50	217.25	30.75	1.01
ODYSSEY	1.35	202.09	268.74	82.24	1.44
ULYSSES	14.4	78.50	305.76	119.26	4.91
		29 May, 0105 UT (ϕ_{Flare} = 203.40°)			
SOHO	−1.0	172.40	219.15	15.75	1.01
ODYSSEY	1.46	203.26	269.91	66.51	1.44
ULYSSES	14.3	78.50	306.22	102.82	4.92
		31 May, 0224 UT (ϕ_{Flare} = 232.40°)			
SOHO	−0.8	173.40	220.15	12.25	1.01
ODYSSEY	1.51	203.84	270.50	38.10	1.44
ULYSSES	14.2	78.50	306.22	73.82	4.92

planetary coronal mass ejections (ICMEs) measured at Ulysses, *Ebert et al.* [2009] identified two consequent ICME plasma structures on 8 June (DOY 159) at 1500 UT and 12 June (DOY 163) at 0800 UT. The time difference between the SEPs onset at Ulysses in this study (DOY ~149 0000 UT) and the first observed ICME plasma structure at Ulysses (DOY 159 15 UT) is ~10.5 days, which is ~4 days less than the estimated travel time of this ICME to Ulysses. Moreover, the simultaneous observations of SEP enhancements at energies exceeding 100 MeV at 1 AU, Mars, and Ulysses suggest that these observations are generated from the same solar event. In section 5, we summarize the timeline of events and describe SEP observations at Earth, Mars, and Ulysses.

[22] An intense X1.6 flare occurred in an active region around 2307 UT on 27 May. The flare was followed by a relatively slow (<1000 km/s) halo CME that was observed at 2355 by SOHO/LASCO coronagraph. On 28 May 0007 UT, a more intense X3.6 flare was observed, followed 13 min later by a fast (1366 km/s) halo CME.

[23] Energetic particle (>20 MeV) enhancements were first observed at SOHO/ERNE around ~2345 UT on 27 May (DOY 147), about 38 min after the first observation of the CME and consistent with the time needed for such particles with these speeds to propagate from the Sun to 1 AU along the Parker spiral. At about ~1200 UT on 29 May (DOY 149), ion intensities (>20 MeV) peaked for about 6 h (following a slow rise) in association with the passage of two IP shocks (S1 and S2), signifying the occurrence of an energetic storm particle (ESP) event [*Cohen et al.*, 2005]. On 29 May at 0105 UT, a third X1.2 flare occurred in the same active region, followed by a fast halo CME that was observed by LASCO at 0127 UT. At 1 AU, a third IP shock (S3) accompanied with proton enhancements arrived at ACE on 30 May at 1600 UT. Although the SEP intensities at 1 AU were already elevated due to the previous particle enhancements, an ESP peak associated with this shock is observed. On 31 May around 0224 UT, a fourth M9.3 flare occurred in the same active region (which had already moved further west on the solar disc) and was associated with a very fast (1835 km/s) halo CME directed toward Earth, which appeared in LASCO at 0230 UT. Shortly after, an abrupt intense SEP enhancement was observed around 0340 UT at 1 AU with no signature of an IP shock. This is the second main peak shown in Figure 1c. The red trace in Figure 1c shows particle observations at Mars during this period as measured by MARIE. Differential intensities are derived from the count rates of two sensors, A1 (responds to protons > 16 MeV) and A2 (measures > 27 MeV protons). The high apparent background is an

Figure 1. (a) Location of Earth (SOHO), Mars (Odyssey), and Ulysses in heliographic coordinates on 28 May 0000 UT (DOY 148), looking down from the north pole at the ecliptic plane. Solid spiral arms represent the nominal magnetic field lines connecting each observer to the Sun, and the dashed lines represent the magnetic field lines connected to the active regions responsible for the four flares, whose X-ray-associated locations on the solar disc with respect to Earth are also shown. The dashed circle represents the Earth orbit. (b) Relative locations of Earth, Mars, and Ulysses on a partial Mollweide projection of the Sun with respect to the Sun-Earth line during the 4 day period. Source surface magnetic field configuration is indicated by red, blue, and black lines, obtained by Wilcox observatory. Solid symbols are different observers' projections on the Sun. Open symbols are the footprints of the magnetic field lines connecting each of them. Active region locations responsible for all flares are shown in orange. The black horizontal arrow depicts the motion of active region AR365 on the Sun during this period. (c) Proton intensities at comparable energies as measured by instruments onboard SOHO (ERNE), Odyssey (MARIE), and Ulysses (COSPIN/HET) during the period from 26 May to 14 June. Black vertical arrows mark the IP shocks observed at 1 AU by the ACE spacecraft magnetometer. The orange arrow points to a possible IP shock at Odyssey. Yellow-shaded box highlights the SEP event arrival at Ulysses (see text for details).

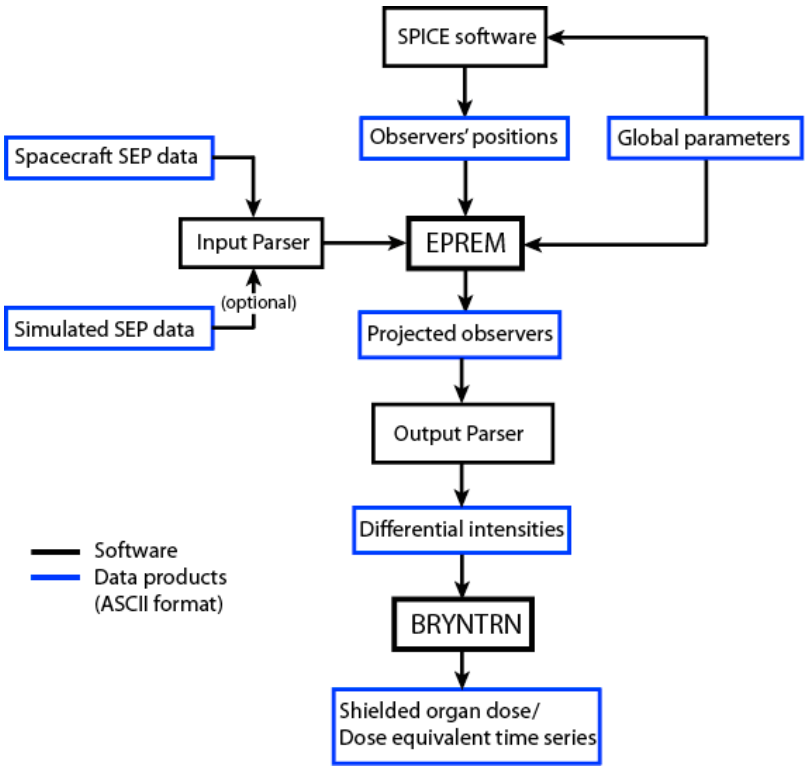

Figure 2. A schematic that illustrates the EMMREM framework.

artifact because A1 counts are always larger than A2, which is more shielded because of its location in the instrument. The recurrent data gaps are due to telemetry-related operations. The intensity profile shows a continuous gradual enhancement which rises faintly above the background starting on 28 May (DOY 148), coinciding with the expected onset of the first SEP. However, this enhancement is only about a factor of 2 above the background at its peak, making it impossible to ascertain whether it is real or instrumental. A sharp short-lived spike structure occurred on 30 May (DOY 150) and was followed by an SEP-like decaying profile (DOY 150.1–151). The decay is interrupted by an abrupt spike (pointed at by the orange arrow) that is consistent with the expected arrival time of shock S2 observed earlier at 1 AU.

[24] Figure 1c also shows Ulysses proton data as measured by COSPIN/LET at 14.5–41.17 MeV during the same period (green trace). LET sensor responds mainly to GCRs, but during intense solar activity, it also responds to solar particles. Under nominal conditions, ~25 MeV particles propagate from Earth to Ulysses in ~7 h along the Parker spiral (assuming free streaming of particles). However, particle signatures of the SEP events appear at Ulysses after ~8 h from their expected arrival in a form of a small peak lasting ~8 h (yellow-shaded box), followed by the main SEP gradual enhancement. An examination of the plasma properties during this period (not shown) reveals a sector boundary around 28 May (DOY 148), which could explain the delayed arrival of particles [see also *Lario et al.*, 2001, 2008]. We note that the 8 h lasting peak lies in a ~1day decrease in the intensity below the preevent GCR background (yellow-shaded box). We remark that since the ~25 MeV intensities are derived from the count rates after subtracting the background, this decrease could be an artifact from the background correction process. Intensities at Ulysses continue to increase gradually for ~24 h (DOY 149–150) and reach a plateau that lasts about 10 days, intensities during these 10 days fluctuate by a factor of 3 and peak around 4 June 1200 UT (DOY 155.5). This peak is also observed in other energy ranges (52 MeV, not shown in Figure 1c), perhaps indicative of a separation between the two isolated SEP events that were observed earlier at 1 AU. The intensities decay back to preevent background levels in about ~3 days, starting from 6 June (DOY 157) to 9 June (DOY 160).

5. Earth-Moon-Mars Radiation Environment Module

[25] The EMMREM project is specifically aimed at predicting real time particle intensities in the heliosphere. It is an evolving project and is currently capable of ingesting 1 AU particle measurements and projecting them to different locations in the heliosphere along the Parker spiral.

[26] Figure 2 schematically illustrates the EMMREM framework. The *Input Parser* converts time series energetic

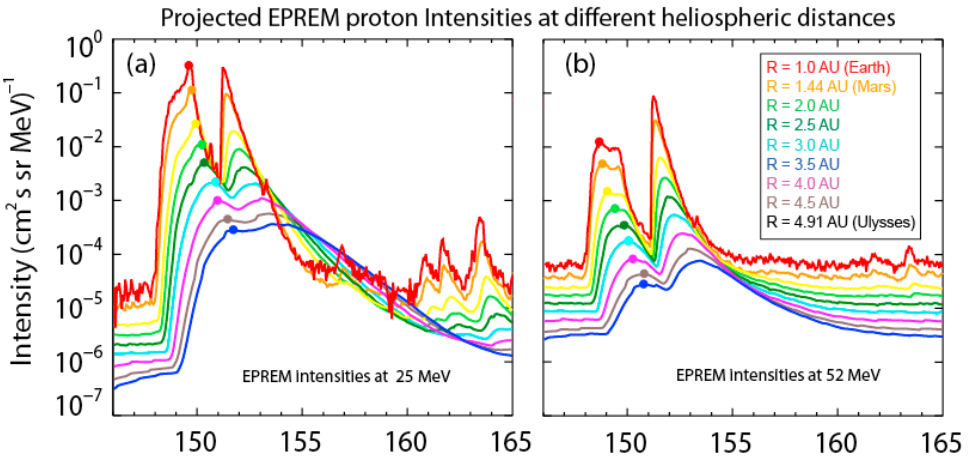

Figure 3. EPREM projected proton intensities of the 27–31 May SEP events at (a) 25 MeV and (b) 52 MeV throughout the heliosphere (1–4.91 AU). Observers are located along the Ulysses magnetic field line at different radial distances. Solid circles represent the peak intensities of the first SEP event at different locations.

particle data (either artificial or measured by spacecraft like GOES, ACE, SOHO, etc.) into an ingestible EMMREM format (distribution function time series). The *Global Input* provides the initialization parameters for the transport code (start and stop times of the event, inner and outer boundaries, mean free path, perpendicular-to-parallel diffusion coefficient ratio, source distribution angle, number of observers, etc.), and the *SPICE* toolkit returns the observer positions in an ingestible ASCII format. The major two parts of EMMREM are (1) the EPREM and (2) the BRYNTRN, which are described briefly below.

[27] EPREM is a transport code that traces particles injected at the inner boundary along magnetic field lines as they are carried out with the solar wind flow. Along each field line, it solves for particle transport, adiabatic focusing, adiabatic cooling, convection, pitch angle scattering, and stochastic acceleration according to the formalism introduced by *Kóta et al.* [2005]. Transport and energy change are treated via a slightly modified form of the focused transport equation [*Skilling*, 1971; *Ruffolo*, 1995; *Tylka*, 2001; *Ng et al.*, 2003], however the coefficients are specified so they can be computed along nodes that move with the solar wind flow:

$$\left(1-\frac{V.\hat{e}_b v\mu}{c^2}\right)\frac{df}{dt}+v\mu\hat{e}_b.\nabla F + \frac{(1-\mu^2)}{2}\left[v\hat{e}_b.\nabla\ln B-\frac{2}{v}\hat{e}_b.\frac{dV}{dt}+\mu\frac{d\ln(nr/B^3)}{dt}\right]\frac{\partial f}{\partial\mu} + \left[-\frac{\mu\hat{e}_b}{v}.\frac{dV}{dt}+\mu^2\frac{d\ln(n/B)}{dt}+\frac{1-\mu^2}{2}\frac{d\ln B}{dt}\right]\frac{\partial f}{\partial\ln p} = \frac{\partial}{\partial\mu}\left(\frac{D_{\mu\mu}}{2}\frac{\partial f}{\partial\mu}\right)-\frac{1}{p^2}\frac{\partial}{\partial p}\left(p^2D_{pp}\frac{\partial f_0}{\partial p}\right). \quad (1)$$

Here v is the particle speed measured in the frame comoving with the solar wind at velocity V, $\hat{e}_b$ is the unit vector along the magnetic field, μ is the cosine of the pitch angle, n is the solar wind density, B is the magnetic field strength, p is the ion momentum, the pitch angle diffusion coefficient is given by

$$D_{\mu\mu}=\left(\frac{R_1}{r}\right)^{3/2}\frac{(1-\mu^2)v}{2\lambda_0}, \quad (2)$$

where the parallel mean free path at $R_1 = 1AU$ is λ_0, and the coefficient associated with diffusion of particle speed is

$$\frac{D_{pp}}{p^2}=\eta^2 D_0 v/V. \quad (3)$$

Here, the ensemble averaged square of the longitudinal field variations is $\eta^2 = \langle(B - B_0)^2/B_0^2\rangle$, where B_0 is the mean magnetic field. The coefficient D_0 characterizes the rate of stochastic acceleration. A detailed description of EPREM formalism is found in the work by *Schwadron et al.* [2010], from which the above description has been acquired.

[28] In order to estimate the radiation hazards at different observer locations, EPREM projected fluxes are fed into the BRYNTRN submodule, after being translated into the correct format through the output parser, as illustrated in Figure 2.

[29] The BRYNTRN submodule [*Wilson et al.*, 1988, 1991] is a deterministic, coupled neutron-proton space radiation code that transports incident spectra (of protons and their secondary products, neutrons, deuterons, tritons, hellions, and alphas) through different aluminum shielding thicknesses and water depths to simulate the dose exposure at different parts of the human body (see *PourArsalan et al.*

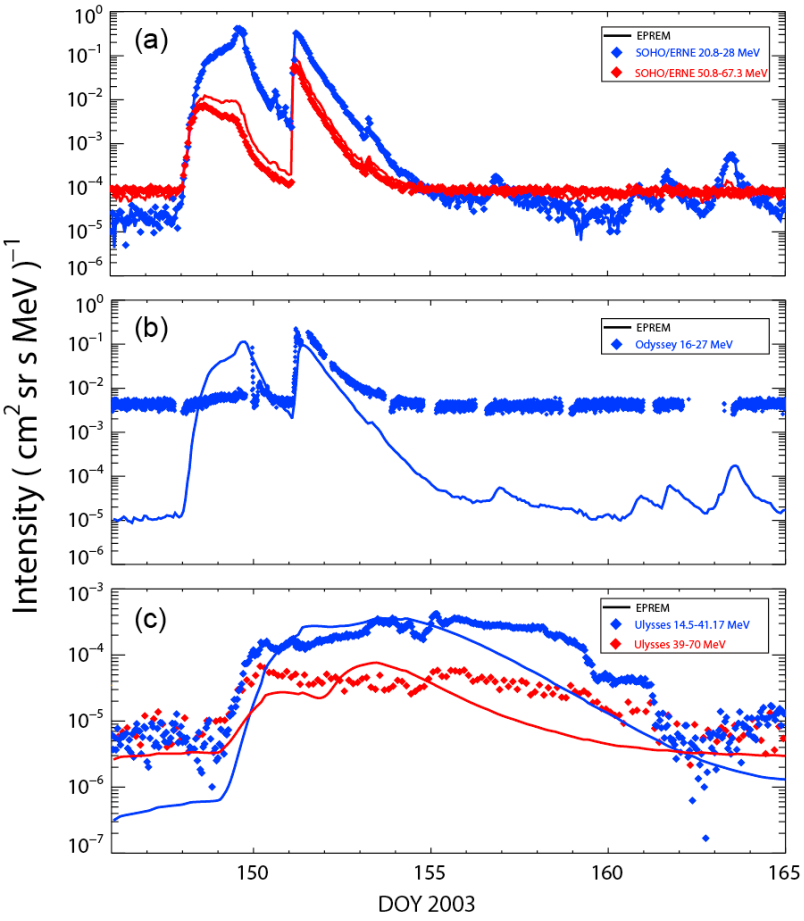

Figure 4. Comparison between observations and EPREM projections of proton intensities at comparable energies at (a) Earth, (b) Mars, and (c) Ulysses. As shown, EPREM is in excellent agreement with observed data at the three different locations.

[2010] for more details). We remark that EPREM transport code does not account for the GCR contributions at larger heliospheric distances, however, this effect is accounted for in the BRYNTRN submodule using the Badhwar-O'Neill GCR model [*O'Neill*, 2006].

6. Modeling the 27–31 May 2003 SEP Events Using EMMREM

6.1. EPREM Setup

[30] EPREM simulation grid consists of individual nodes that convect radially with the solar wind to form the Parker spiral pattern. We have used a measured solar wind speed of 500 km/s to drive the simulation grid nodes from an inner boundary of 0.99 AU to a converging point of 5.8 AU. The inner boundary was populated by proton intensities measured by SOHO/ERNE at energies between ~1.5 MeV and ~130 MeV, in 20 different energy ranges. These small energy steps provided a high-resolution input so that the interpolation between intensities at different energies yielded minimal errors. Particles are injected isotropically along all field lines within 100° on each side of the Earth. In order to examine the intensities at different locations, we have planted virtual observers along the same field line but at seven different radial distances (2, 2.5, 3, 3.5, 4, and 4.5), in addition to three fixed observers corresponding to Earth (1 AU), Mars (1.44 AU), and Ulysses (4.91 AU). Throughout the simulation, we assume a diffusion-coefficient ratio ($\kappa_\perp/\kappa_{||}$) of 0.05 and a parallel scattering mean free path ($\lambda_{||}$) that is proportional to particle rigidity to the 1/3 power, scaled by a fixed value of 0.01 AU at 1 GV rigidity. We remark that this form of $\lambda_{||}$ is fixed throughout the simulation and does not vary with radial distance [e.g., *Li et al.*, 2003].

[31] We tried several runs using different values for both $\kappa_\perp/\kappa_{||}$ and $\lambda_{||}$, we found that our selected values yielded the best agreement with data at both Mars and Ulysses for this event. We remark that decreasing $\kappa_\perp/\kappa_{||}$ to 0.01 and changing $\lambda_{||}$ to 0.05 AU did not have a significant effect on the result. However, the effects of varying the transport parameters on the results will not be discussed in this paper. It is worth mentioning that the value of $\lambda_{||}$ used

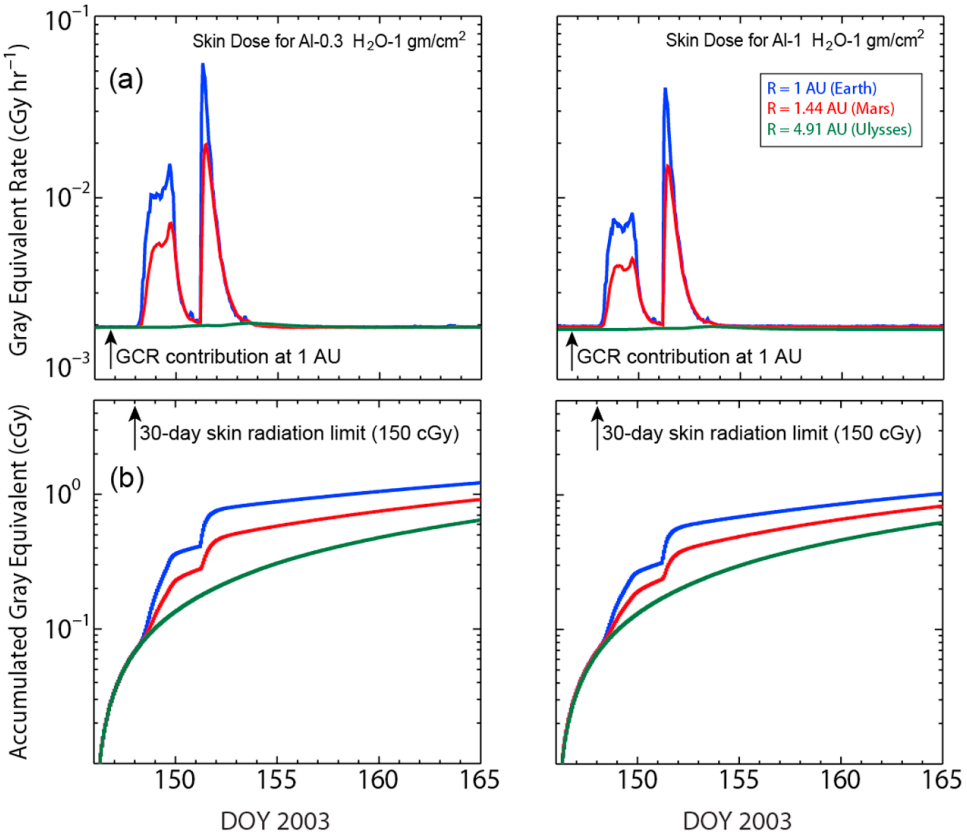

Figure 5. BRYNTRN calculations of (a) the skin gray equivalent rates and (b) the cumulative gray equivalent for two different shielding thicknesses at Earth, Mars, and Ulysses. The background level represents the dose contribution from GCRs at 1 AU.

here is slightly lower than the observed values (0.08–0.3 AU) for most solar events [see *Kallenrode*, 2005; *Giacalone*, 1998, and references therein].

6.2. Proton Intensities Across the Heliosphere: Data Versus EPREM

[32] Figure 3 shows proton intensities projected by EPREM to different radial distances between 1 and 4.91 AU at 25 MeV (Figure 3a) and 52 MeV (Figure 3b). Color-coded circles represent the peak intensities at different locations. In both panels, peak intensities correspond only to the first SEP event. We have chosen to study the peak gradients in the first event to insure quiet preevent periods at different locations. Figure 4 shows a comparison of proton measurements and EPREM intensities at Earth (SOHO), Mars (Odyssey), and Ulysses at similar energy ranges of ~25 MeV (three locations) and ~52 MeV (Earth and Ulysses). As shown, there is very good agreement between time onsets and temporal profiles at all locations and at different energies (except for the first event on Mars). We note that the agreement at Earth is natural since the projection is very close to the inner boundary. However, at further distances, the projection of particles depends partially on the interplanetary conditions and the initial parameters (such as the mean free path, diffusion coefficients, solar wind speed, etc.). We have observed from different runs that variations in these parameters (within a reasonable range) lead to slightly different results at different distances. This effect can be seen at the ~25 MeV channel at Ulysses in Figure 4c, where the event decays faster than what the data reveals, possibly indicating an enhanced diffusion coefficients ratio.

6.3. Dose and Dose Equivalents

[33] Figure 5 shows the gray equivalent rates (Figure 5a) and the accumulated gray equivalent (Figure 5b) of the SEP events assuming the GCR contribution level at 1 AU. We have subtracted the contribution of GCRs beyond 1 AU (which increases with increasing radial distance) in order to quantify the sole SEP contribution to the radiation exposure. Since we are interested in the effects of radiation from a biological perspective, it is reasonable to discuss the absorbed dose, which is measured in gray (Gy). Radiation Dose is a quantity equivalent to the energy deposited by incoming radiation in a material or tissue per unit mass (1 gray = 1 J/kg). Gray equivalent (DE) is used to

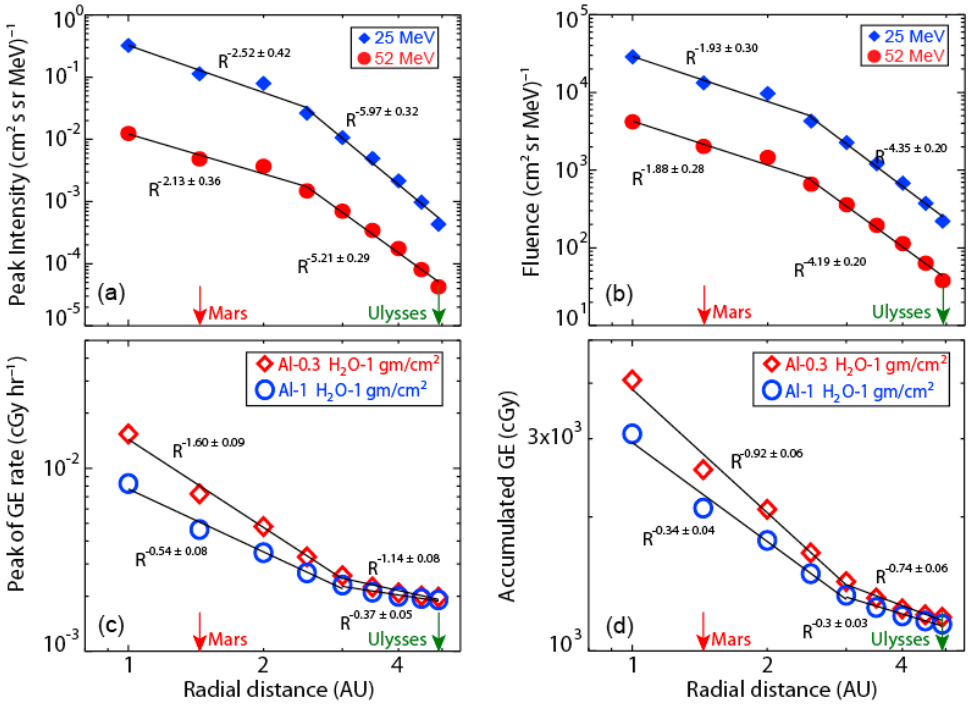

Figure 6. EPREM radial gradients of (a) peak intensities (first SEP event) and (b) fluences (both events) at 25 MeV and 52 MeV between 1 and 4.91 AU. (c) Radial gradients of corresponding peak dose equivalent rates and (d) integrated dose equivalent at different locations. In both Figures 6c and 6d, solid lines represent power law fits.

quantify the short-term radiation effects on humans from penetrating protons. It is defined as

$$\mathrm{DE}(\mathrm{Gy_{eq}}) = \mathrm{D}(\mathrm{Gy}) \times \mathrm{RBE},$$

where D is the dose in gray and RBE is the relative biological effectiveness, which is a measure of how damaging the radiation is when compared to X-rays. For SEPs, which mostly consist of protons, this value is set to be 1.5. SEP heavy ions are not usually a major contributor to the dose and dose equivalent behind shielding, since their spectra are much softer than those of protons. We remark that target recoil doses are accounted for within the code and are not a major dose contributor as well.

[34] The BRYNTRN submodule converts particle intensities into dose and dose equivalents [see *Wilson et al.*, 1991] using different aluminum shielding and depths of water. We have used aluminum thicknesses of 0.3 g/cm^2 and 1.0 g/cm^2 that correspond to a nominal spacesuit and a thick spacesuit, respectively. Water thickness of 1.0 g/cm^2 was used to surrogate the human skin [see *PourArsalan et al.*, 2010].

7. Radial Dependence of Peak Intensities, Fluences, and Dose Equivalents

[35] We have used EMMREM outputs at all observers to examine the radial gradients of particle peak intensities, fluences, and radiation doses at nine different locations from 1 to 4.91 AU. Figure 6a shows the radial dependence of peak proton intensities of the first SEP event at 25 MeV (blue diamonds) and 52 MeV (red circles). Radial dependence of fluences from both events at the two energies is shown in Figure 6b. Peak intensities are those corresponding to the first SEP event and represent the maximum value of the proton intensity at each observer and at each energy. A broken power law is observed in the radial dependencies of both the peak intensities and fluences, with a break at ~2.5 AU. Figures 6c and 6d show the radial dependence of DE rates and the integrated DE at each location. A break is also observed at ~3 AU. Fit parameters corresponding to the radial dependencies of these quantities are summarized in Table 3 (peak intensities and fluences) and Table 4 (DE and integrated DE).

8. Discussion and Conclusions

[36] We have used the EMMREM model to study the radial gradients of proton intensities (at 25 and 52 MeV)

Table 3. Radial Dependence of Peak Intensities and Fluences Between 1 and 4.91 AU

	~25 MeV		~52 MeV	
Distance	Peak Intensities	Fluences	Peak Intensities	Fluences
1–2.5 AU	$R^{-2.52 \pm 0.42}$	$R^{-1.93 \pm 0.30}$	$R^{-2.13 \pm 0.36}$	$R^{-1.88 \pm 0.28}$
>2.5 AU	$R^{-5.97 \pm 0.32}$	$R^{-4.35 \pm 0.20}$	$R^{-5.21 \pm 0.29}$	$R^{-4.19 \pm 0.20}$

Table 4. Radial Dependence of DE Rates and Integrated DE Between 1 and 4.91 AU

	Al = 0.3; H_2O = 1.0 (gm/cm^2)		Al = 1.0; H_2O = 1.0 (gm/cm^2)	
Distance	Peak DE Rates	Integrated DE Rates	Peak Intensities	Fluences
1–3.0 AU	$R^{-1.60 \pm 0.09}$	$R^{-0.92 \pm 0.06}$	$R^{-0.54 \pm 0.08}$	$R^{-0.34 \pm 0.04}$
>3.0 AU	$R^{-1.14 \pm 0.08}$	$R^{-0.74 \pm 0.06}$	$R^{-0.37 \pm 0.05}$	$R^{-0.30 \pm 0.03}$

and corresponding radiation dose exposures at different locations in the heliosphere during the 27–31 May 2003 SEP events. On the Sun, an active region produced four major flares with the first flare located at W19 and the last one at W59. This period was associated with two main SEP events that were observed by multi spacecraft at 1 AU, with enhanced SEP intensities that lasted for about 7 days. The same events were shortly thereafter observed at Mars and by Ulysses located at 1.44 AU and 4.91 AU, respectively.

[37] As shown in Figures 1a and 1b, all flares and observers were located within a narrow latitudinal range close to the ecliptic plane. Longitudinally, Earth and Mars were relatively close to the flare locations, both in heliolongitude and their MFL footprints at the Sun, while Ulysses was significantly farther away, with the smallest MFL footprint separation being ~74° from the last flare F4. However, both events were observed at Ulysses and at different energy ranges. The typical longitudinal widths of CMEs are ~45°–90° [*Hundhausen*, 1993; *Zhang et al.*, 2009] and while this could explain the second SEP event at Ulysses, it does not account for the first event, where the MFL footprint of Ulysses was ~120° away from the flare source. Since the first event was associated with a strong IP shock, another scenario is possible: the associated IP shock populated the field lines with accelerated particles as it propagated radially in the heliosphere, and thus enabling particles to be observed at Ulysses even though its connected MFL was not originally populated with particles near the Sun. However, it is unlikely that all the SEPs observed at Ulysses are due to the single IP shock, because of the large enhancements that lasted for more than 10 days and the time profiles are consistent with two SEP events that appear to have merged together. Moreover, if the shock was the reason for particles to appear at Ulysses, any magnetic disconnectivity within the shock region would have largely affected the SEP time profiles at Ulysses. We note that during long-lasting (~7 days at 1 AU) SEP events like the 27–31 May case, Ulysses spacecraft samples field lines that are rooted over a wide longitudinal extent on the Sun, exceeding 100° [see also *Zhang et al.*, 2009]. This effect, along with the radially moving IP shock, has contributed to populating the field lines connected to Ulysses, leading to the observed temporal profile discussed above.

[38] This analysis raises an important issue: If EPREM does not account for GCRs and IP shock acceleration, why are the EPREM projected SEP profiles at Ulysses in such a good agreement with SEP measurements? Two scenarios could provide an answer to this. First, since EPREM is a transport code, it does not really matter what the input profiles are, as long as they are distributed over a wide range of field lines with one of them connected to the observer of interest. The only effect that could alter the time profiles is the cross-field diffusion from the neighboring eastern corotating field lines. Second, if the IP shock is poorly accelerating particles beyond 1 AU [e.g., *Zank et al.*, 2000; *Li et al.*, 2003], it will not have a significant effect on the SEP profiles at larger distances, especially at high energies as in this study (25 MeV and 52 MeV).

[39] As summarized in Table 3, the radial dependences of proton peak intensities and event fluences exhibit power laws that are harder (1 to ~2.5 AU) and softer (~2.5 to 4.91 AU) than those recommended for radial extrapolations beyond 1 AU [*Feynman and Gabriel*, 1988]. Using the EPREM submodule coupled with an MHD code, *Kozarev et al.* [2010] studied the radial gradients of peak intensities and fluences of the Halloween SEP events [*Lario et al.*, 2005] at 1, 1.5, 3, and 5 AU. For protons at ~52 MeV, they found that radial dependence of event fluence vary as a single power law of index -3.83 ± 0.32, this value is slightly higher then the recommendations by *Feynman and Gabriel* [1988]. The fact that this value falls between our values of the broken power law indices at similar energy (-1.88 ± 0.28 (1 to 2.5 AU) and -4.19 ± 0.20 (2.5 to 4.91 AU)) indicates that the broken law could be the case for the Halloween event as well. However, the lack of fluence-deduced values at more radial distances makes it hard to confirm that this is indeed the case. We note that the comparison of the peak intensity gradients between our results and those obtained by Kozarev et al. is not relevant, since they studied the peak gradients of all the Halloween SEP cluster as it propagated in the IP space, and thus could largely be altered by contributions from individual SEP events. Fluence comparison is more immune to this effect, since the bulk of particles move together.

[40] The break observed in the radial dependence is probably because at large radial distances, the Parker spiral becomes very toroidal and the transport of particles along the magnetic field lines becomes less effective than transport across field lines. In other words, the angle between the magnetic field line and the radial velocity vector becomes very large, decreasing the effectiveness of radial transport and increasing the intensity gradient.

[41] BRYNTRN calculation of radiation doses during this period showed that the event posed no imminent risk to humans in the IP space environment, with cumulative DE less than the 30 day skin limits by more than an order of magnitude. Beyond ~3 AU, radiation doses of these events became comparable to the GCR contribution in the Earth vicinity. The spectral break (ankle) observed in Figures 6c and 6d would probably disappear if the event was stronger, as in the case of the 2003 Halloween SEP events [see *Kozarev et al.*, 2010].

[42] In summary, we have shown that the EMMREM model can reproduce SEP intensities that agree well with

measurements at different locations between 1 and 4.91 AU. At large radial distances, SEPs are observed over wide longitudinal widths to include regions that are not magnetically connected to the SEP source region at the Sun, possibly indicating large CME sizes and/or high cross-field diffusion at large radial distances. Nonetheless, we emphasize that EPREM solves for particle transport and does not take into account the radially expanding, CME-driven, IP shock often associated with SEP events. This limitation omits a possible movable source of particles that could be significant in populating the magnetic field lines with shock-accelerated particles at small radial distances (~1 AU and less). Radial dependences of proton peak intensities exhibit a broken power law between 1 to 2.5 AU and 2.5 to 4.91 AU, ranging between $R^{-2.52 \pm 0.42}$ and $R^{-5.97 \pm 0.32}$ for 25 MeV and between $R^{-2.13 \pm 0.36}$ and $R^{-5.21 \pm 0.29}$ for 52 MeV. Event fluences exhibit a similar behavior but with a harder spectra. Dependencies up to ~2.5 AU are harder than those deduced from earlier diffusion models. The results appear to be consistent with those of a different study for an intense SEP period (2003 SEP Halloween events) using EMMREM. Nonetheless, the radial dependence of SEP events needs to be revisited and examined using more observers and different SEP events. Radiation dose calculations show that these events did not pose a short-term radiation hazard to humans in the IP space.

[43] **Acknowledgments.** We are grateful to the Ulysses Data System, the ACE Science Center, and the Odyssey/MARIE, SOHO/ERNE, and Ulysses/COSPIN instrument teams for providing the data sets for this study. We acknowledge the use of ACE/SWOOPS, MAG, and Ulysses/SWEPAM, MAG, and the SOHO/LASCO in our analysis. M.A.D. thanks R. B. McKibben for providing PHA and count rates data from the Ulysses COSPIN/HET instrument. The work at Southwest Research Institute was supported by NASA research grant NNX07AC12G.

References

Aran, A., B. Sanahuja, and D. Lario (2005a), A first step towards proton flux forecasting, *Adv. Space Res.*, *36*, 2333, doi:10.1016/j.asr.2004.06.023.

Aran, A., B. Sanahuja, and D. Lario (2005b), Fluxes and fluences of SEP events derived from SOLPENCO, *Ann. Geophys.*, *23*(9), 3047.

Balogh, A., T. J. Beek, R. J. Forsyth, P. C. Hedgecock, R. J. Marquedant, E. J. Smith, D. J. Southwood, and B. T. Tsurutani (1992), The magnetic field investigation on the ULYSSES mission—Instrumentation and preliminary scientific results, *Astron. Astrophys. Suppl. Ser.*, *92*, 221.

Bame, S. J., J. L. Phillips, D. J. McComas, J. T. Gosling, and B. E. Goldstein (1992), The ULYSSES solar wind plasma investigation—Experiment description and initial in-ecliptic results, in *Solar Wind Seven*, edited by E. Marsch and R. Schwenn, p. 139, Elsevier, New York.

Barouch, E., and L. F. Burlaga (1976), Three-dimensional interplanetary stream magnetism and energetic particle motion, *J. Geophys. Res.*, *81*, 2103, doi:10.1029/JA081i013p02103.

Boufaida, M., and T. P. Armstrong (1997), Spatial variations of 0.2 to 5 MeV protons in the 1–5 AU in-ecliptic region from Ulysses, Voyager 1 and 2, and IMP 8 gradient studies, *J. Geophys. Res.*, *102*, 7013, doi:10.1029/97JA00135.

Burlaga, L. F., S. P. Plunkett, and O. C. St. Cyr (2002), Successive CMEs and complex ejecta, *J. Geophys. Res.*, *107*(A10), 1266, doi:10.1029/2001JA000255.

Chae, J., Y. Moon, and Y. Park (2004), Determination of magnetic helicity content of solar active regions from SOHO/MDI magnetograms, *Sol. Phys.*, *223*, 39, doi:10.1007/s11207-004-0938-9.

Cohen, C. M. S., R. A. Mewaldt, C. W. Smith, R. M. Skoug, G. C. Ho, and A. Szaboe (2005), Energetic particle responses to interplanetary shocks observed by ACE, in *Proceedings of the 29th International Cosmic Ray Conference*, vol. 1, edited by B. Sripathi Acharya et al., p. 327, Tate Inst. of Fundam. Res., Mumbai, India.

Cucinotta, F. A., W. Schimmerling, J. W. Wilson, L. E. Peterson, G. D. Badhwar, P. B. Saganti, and J. F. Dicello (2001), Space radiation cancer risks and uncertainties for Mars missions, *Radiat. Res.*, *156*(5), 682.

Denker, C., J. Z. Reza, A. J. Nelson, J. D. Patterson, T. P. Armstrong, C. G. Maclennan, and L. J. Lanzerotti (2007), Statistical study of low-energy heliosphere particle fluxes from 1.4 to 5 AU over a solar cycle, *Space Weather*, *5*, S07002, doi:10.1029/2006SW000274.

Ebert, R. W., D. J. McComas, H. A. Elliott, R. J. Forsyth, and J. T. Gosling (2009), Bulk properties of the slow and fast solar wind and interplanetary coronal mass ejections measured by Ulysses: Three polar orbits of observations, *J. Geophys. Res.*, *114*, A01109, doi:10.1029/2008JA013631.

Feynman, J., and S. Gabriel (1988), *Interplanetary Particle Environment: Proceedings of a Conference*, *JPL Publ.*, 88-28.

Fisk, L. A., and J. R. Jokipii (1999), Mechanisms for latitudinal transport of energetic particles in the heliosphere, *Space Sci. Rev.*, *89*, 115, doi:10.1023/A:1005285003239.

Foullon, C., N. Crosby, and D. Heynderickx (2005), Toward interplanetary space weather: Strategies for manned missions to Mars, *Space Weather*, *3*, S07004, doi:10.1029/2004SW000134.

Giacalone, J. (1998), Cosmic ray transport coefficients, *Space Sci. Rev.*, *83*, 351, doi:10.1023/A:1005087326666.

Gopalswamy, N., S. Yashiro, G. Michalek, G. Stenborg, A. Vourlidas, S. Freeland, and R. Howard (2009), The SOHO/LASCO CME catalog, *Earth Moon Planets*, *104*, 295, doi:10.1007/s11038-008-9282-7.

Hamilton, D. C. (1988), The radial dependence of the solar energetic particle flux, in *Interplanetary Particle Environment: Proceedings of a Conference*, edited by J. Feynman and S. Gabriel, *JPL Publ.*, 88-28, 86.

Hamilton, D. C., G. M. Mason, and F. B. McDonald (1990), The radial dependence of the peak flux and fluence in solar energetic particle events, in *Proceedings of the 21st International Cosmic Ray Conference*, vol. 5, edited by R. J. Protheroe, p. 237, Univ. of Adelaide, Adelaide, SA, Australia.

Hanuise, C., et al. (2006), From the Sun to the Earth: Impact of the 27–28 May 2003 solar events on the magnetosphere, ionosphere and thermosphere, *Ann. Geophys.*, *24*(1), 129.

Hundhausen, A. J. (1993), Sizes and locations of coronal mass ejections: SMM observations from 1980 and 1984–1989, *J. Geophys. Res.*, *98*, 13,177, doi:10.1029/93JA00157.

Kallenrode, M.-B. (1993), Particle propagation in the inner heliosphere, *J. Geophys. Res.*, *98*, 19,037, doi:10.1029/93JA02079.

Kallenrode, M.-B. (2005), Radial dependence of solar energetic particle events, in *"Connecting Sun and Heliosphere": Proceedings of Solar Wind 11/SOHO 16*, edited by B. Fleck and T. H. Zurbuchen, *Eur. Space Agency Spec. Publ.*, *ESA SP592*, 87.

Kóta, J., W. B. Manchester, and T. I. Gombosi (2005), SEP acceleration at realistic CMEs: Two sites of acceleration?, in *Proceedings of the 29th International Cosmic Ray Conference*, vol. 1, edited by B. Sripathi Acharya et al., p. 125, Tate Inst. of Fundam. Res., Mumbai, India.

Kozarev, K., N. A. Schwadron, M. A. Dayeh, L. W. Townsend, M. I. Desai, and M. PourArsalan (2010), *Modeling the 2003 Halloween events with EMMREM: Energetic particles*, radial gradients, and coupling to MHD, *Space Weather*, doi:10.1029/2009SW000550, in press.

Lario, D., D. K. Haggerty, E. C. Roelof, S. J. Tappin, R. J. Forsyth, and J. T. Gosling (2001), Joint Ulysses and ACE observations of a magnetic cloud and the associated solar energetic particle event, *Space Sci. Rev.*, *97*, 277, doi:10.1023/A:1011829101277.

Lario, D., R. B. Decker, S. Livi, S. M. Krimigis, E. C. Roelof, C. T. Russell, and C. D. Fry (2005), Heliospheric energetic particle observations during the October–November 2003 events, *J. Geophys. Res.*, *110*, A09S11, doi:10.1029/2004JA010940.

Lario, D., et al. (2006), Radial and longitudinal dependence of solar 4–13 MeV and 27–37 MeV proton peak intensities and fluences: Helios and IMP 8 observations, *Astrophys. J.*, *653*, 1531, doi:10.1086/508982.

Lario, D., A. Aran, N. Agueda, and B. Sanahuja (2007), Radial dependence of proton peak intensities and fluences in SEP events: Influence of the energetic particle transport parameters, *Adv. Space Res.*, *40*, 289, doi:10.1016/j.asr.2007.01.057.

Lario, D., A. Aran, and R. B. Decker (2008), Major solar energetic particle events of solar cycles 22 and 23: Intensities above the streaming limit, *Space Weather*, *6*, S12001, doi:10.1029/2008SW000403.

Le Roux, J. A., and M. S. Potgieter (1995), The simulation of complete 11 and 12 year modulation cycles for cosmic rays in the heliosphere using a drift model with global merged interaction regions, *Astrophys. J.*, *442*, 847, doi:10.1086/175487.

Li, G., G. P. Zank, and W. K. M. Rice (2003), Energetic particle acceleration and transport at coronal mass ejection-driven shocks, *J. Geophys. Res.*, *108*(A2), 1082, doi:10.1029/2002JA009666.

Li, G., G. P. Zank, and W. K. M. Rice (2005), Acceleration and transport of heavy ions at coronal mass ejection-driven shocks, *J. Geophys. Res.*, *110*, A06104, doi:10.1029/2004JA010600.

Luhmann, J. G., S. A. Ledvina, D. Krauss-Varban, D. Odstrcil, and P. Riley (2007), A heliospheric simulation-based approach to SEP source and transport modeling, *Adv. Space Res.40*, 295, doi:10.1016/j.asr.2007.03.089.

McComas, D. J., S. J. Bame, P. Barker, W. C. Feldman, J. L. Phillips, P. Riley, and J. W. Griffee (1998), Solar Wind Electron Proton Alpha Monitor (SWEPAM) for the Advanced Composition Explorer, *Space Sci. Rev.*, *86*, 563.

Mewaldt, R. A., C. M. S. Cohen, D. K. Haggerty, G. M. Mason, M. L. Looper, T. T. von Rosenvinge, and M. E. Wiedenbeck (2007), Radiation risks from large solar energetic particle events, in *Turbulence and Nonlinear Processes in Astrophysical Plasmas: 6th Annual International Astrophysics Conference*, edited by D. Shaikh and G. P. Zank, *AIP Conf. Proc.*, 932, 277.

Ng, C. K., and D. V. Reames (1994), Focused interplanetary transport of approximately 1 MeV solar energetic protons through self-generated Alfven waves, *Astrophys. J.*, *424*, 1032, doi:10.1086/173954.

Ng, C. K., D. V. Reames, and A. J. Tylka (2003), Modeling shock-accelerated solar energetic particles coupled to interplanetary Alfvén waves, *Astrophys. J.*, *591*, 461, doi:10.1086/375293.

O'Neill, P. M. (2006), Badhwar-O'Neill galactic cosmic ray model update based on Advanced Composition Explorer (ACE) energy spectra from 1997 to present, *Adv. Space Res.*, *37*, 1727, doi:10.1016/j.asr.2005.02.001.

Parker, E. N. (1965), The passage of energetic charged particles through interplanetary space, *Planet. Space Sci.*, *13*, 9, doi:10.1016/0032-0633(65)90131-5.

PourArsalan, M., L. W. Townsend, N. A. Schwadron, K. Kozarev, M. A. Dayeh, and M. I. Desai (2010), Time-dependent estimates of organ dose and dose equivalent rates for human crews in deep space from the 26 October 2003 solar energetic particle event (Halloween event) using the Earth-Moon-Mars Radiation Environment Module, *Space Weather*, *8*, S00E05, doi:10.1029/2009SW000533.

Qin, G., and G. Li (2008), Effect of flux tubes in the solar wind on the diffusion of energetic particles, *Astrophys. J.*, *682*, L129, doi:10.1086/591229.

Reames, D. V. (1999), Particle acceleration at the Sun and in the heliosphere, *Space Sci. Rev.*, *90*, 413, doi:10.1023/A:1005105831781.

Reames, D. V. (2001), Energetic particle composition, in *Solar and Galactic Composition: A Joint SOHO/ACE Workshop*, edited by R. F. Wimmer-Schweingruber, *AIP Conf. Proc.*, 598, 153, doi:10.1063/1.1433994.

Rice, W. K. M., G. P. Zank, and G. Li (2003), Particle acceleration and coronal mass ejection driven shocks: Shocks of arbitrary strength, *J. Geophys. Res.*, *108*(A10), 1369, doi:10.1029/2002JA009756.

Richardson, J. D., Y. Liu, C. Wang, and L. F. Burlaga (2006), ICMES at very large distances, *Adv. Space Res.*, *38*, 528, doi:10.1016/j.asr.2005.06.049.

Ruffolo, D. (1995), Effect of adiabatic deceleration on the focused transport of solar cosmic rays, *Astrophys. J.*, *442*, 861, doi:10.1086/175489.

Ruzmaikin, A., G. Li, G. Zank, J. Feynman, and I. Jun (2005), The radial dependence of solar energetic particle fluxes, in *"Connecting Sun and Heliosphere": Proceedings of Solar Wind 11/SOHO 16*, edited by B. Fleck and T. H. Zurbuchen, *Eur. Space Agency Spec. Publ.*, *ESA SP592*, 441.

Sako, T., et al. (2005), Possible >10GeV particle detection in association with the 28 May 2003 solar flare, in *Proceedings of the 29th International Cosmic Ray Conference*, vol. 1, edited by B. Sripathi Acharya et al., p. 21, Tate Inst. of Fundam. Res., Mumbai, India.

Schwadron, N. A., et al. (2010), Earth-Moon-Mars Radiation Environment Module framework, *Space Weather*, *8*, S00E02, doi:10.1029/2009SW000523.

Shea, M. A. (1988), Intensity/time profiles of solar particle events at one astronomical unit, in *Interplanetary Particle Environment: Proceedings of a Conference*, edited by J. Feynman and S. Gabriel, *JPL Publ.*, 88-28, 75.

Simpson, J. A., et al. (1992), The ULYSSES Cosmic Ray and Solar Particle Investigation, *Astron. Astrophys. Suppl. Ser.*, *92*, 365.

Skilling, J. (1971), Cosmic rays in the galaxy: Convection or diffusion?, *Astrophys. J.*, *170*, 265, doi:10.1086/151210.

Smart, D. F., and M. A. Shea (2003), Comment on estimating the solar proton environment that may affect Mars missions, *Adv. Space Res.*, *31*, 45, doi:10.1016/S0273-1177(02)00655-5.

Smith, C. W., J. L'Heureux, N. F. Ness, M. H. Acuña, L. F. Burlaga, and J. Scheifele (1998), The ACE Magnetic Fields Experiment, *Space Sci. Rev.*, *86*, 613, doi:10.1023/A:1005092216668.

Torsti, J., et al. (1995), Energetic particle experiment ERNE, *Sol. Phys.*, *162*, 505, doi:10.1007/BF00733438.

Tylka, A. J. (2001), New insights on solar energetic particles from Wind and ACE, *J. Geophys. Res.*, *106*, 25,333, doi:10.1029/2000JA004028.

Wilson, J. W., L. W. Townsend, S. Y. Chun, W. W. Buck, F. Khan, and F. Cucinotta (1988), BRYNTRN: A baryon transport computer code: Computation procedures and data base, *NASA Tech. Memo.*, *NASA-TM-4037*, 42.

Wilson, J. W., L. W. Townsend, W. S. Schimmerling, G. S. Khandelwal, F. Khan, J. E. Nealy, F. A. Cucinotta, L. C. Simonsen, J. L. Shinn, and J. W. Norbury (1991), Transport methods and interactions for space radiations, *NASA Ref. Publ.*, *NASA-RP-1257*.

Wilson, J. W., L. C. Simonsen, J. L. Shinn, R. R. Dubey, W. Jordan, and M. Kim (1997), Radiation analysis for the Human Lunar Return Mission, *NASA Tech. Pap.*, *NASA-TP-3662*.

Zank, G. P., W. K. M. Rice, and C. C. Wu (2000), Particle acceleration and coronal mass ejection driven shocks: A theoretical model, *J. Geophys. Res.*, *105*, 25,079, doi:10.1029/1999JA000455.

Zeitlin, C., T. Cleghorn, F. Cucinotta, P. Saganti, V. Andersen, K. Lee, L. Pinsky, W. Atwell, R. Turner, and G. Badhwar (2004), Overview of the Martian radiation environment experiment, *Adv. Space Res.*, *33*, 2204, doi:10.1016/S0273-1177(03)00514-3.

Zhang, M., G. Qin, and H. Rassoul (2009), Propagation of solar energetic particles in three-dimensional interplanetary magnetic fields, *Astrophys. J.*, *692*, 109.

M. A. Dayeh and M. I. Desai, Space Science and Engineering Division, Southwest Research Institute, 6220 Culebra Rd., San Antonio, TX 78238, USA. (maldayeh@swri.edu)

R. B. Hatcher, M. PourArsalan, and L. W. Townsend, Department of Nuclear Engineering, University of Tennessee, 215 Pasqua Nuclear Engineering Bldg., 1004 Estabrook Rd., Knoxville, TN 37996, USA.

K. Kozarev, Department of Astronomy, Boston University, 275 Commonwealth Ave., Boston, MA 01760, USA.

N. A. Schwadron, Institute for the Study of Earth, Oceans, and Space, University of New Hampshire, Durham, NH 03824, USA.

C. Zeitlin, Space Studies Department, Southwest Research Institute, 1050 Walnut St., Boulder, CO 80302, USA.